Open Access

Catalysis Research

Research Article

Synthesis of SAPO-34 Zeolite Membrane: Influence of Sources of Silica

Tellys Lins Almeida Barbosa [†], Meiry Gláucia Freire Rodrigues [†,*]

Universidade Federal de Campina Grande, Unidade Acadêmica de Engenharia Química, 58109-970 Campina Grande - PB, Brazil; E-Mails: tellyslins@hotmail.com; meiry.freire@eq.ufcg.edu.br

† These authors contributed equally to this work.

* **Correspondence:** Meiry Gláucia Freire Rodrigues; E-Mail: meiry.freire@eq.ufcg.edu.br

Academic Editor: Angela Martins

Special Issue: Zeolite Materials and Catalysis

Catalysis Research
2023, volume 3, issue 4
doi:10.21926/cr.2304030

Received: October 03, 2023
Accepted: December 05, 2023
Published: December 11, 2023

Abstract

The research described the production and characterization of various materials, particularly alpha-alumina ceramic supports, zeolite SAPO-34, and zeolite membranes. Ceramic supports were manufactured through dry uniaxial compaction. Sintering of the supports was carried out at 1300°C for 2 h. SAPO-34 zeolites and zeolite membranes were synthesized through a hydrothermal process involving two steps: a first step at 38°C for 24 h and a second step at 200°C for 24 h. The research aimed to determine how different silica sources, namely Aerosil 380, colloidal silica, and TEOS, influenced the outcome of the synthesis. The study identified that Aerosil 380 silica was the most suitable source for synthesizing SAPO-34 zeolites and membranes. Zeolite membranes (SAPO-34/alpha-alumina) displayed a uniform and homogeneous distribution of SAPO-34 phase zeolitic crystals. The absence of defects or cracks in these membranes confirmed the successful formation of the SAPO-34 zeolite membrane structure. This research has significant implications, particularly in materials science and applications utilizing zeolites and membranes. The choice of silica source plays a crucial role in determining the quality and properties of the synthesized materials, and the detailed characterization provides valuable insights into their performance in practical applications.

Overall, the research contributes to the understanding and optimization of zeolite synthesis processes.

Keywords
SAPO-34 zeolite synthesis; zeolite membrane; alpha-alumina; hydrothermal method; silica sources

1. Introduction

SAPO-34 is a type of zeolite, a crystalline aluminosilicate material with a well-defined porous structure. It was first discovered at Union Carbide Corporation, and its crystal structure and its analogy with natural chabazite were initially reported by the authors referenced in your statement. Zeolites like SAPO-34 have a wide range of applications due to their unique properties, including their high surface area and molecular sieve capabilities [1-7].

Various methods have been employed to synthesize SAPO molecular sieves, including microwave irradiation, ultrasonic treatment, dry gel conversion, and hydrothermal synthesis [8]. The organic structure directing agent (SDA) plays a crucial role in the crystal growth of SAPOs. The template has been employed in synthesizing SAPO-34, including morpholine, piperidine, diethylamine, triethylamine, isopropylamine, and TEAOH-dipropylamine. These agents can influence the synthesis process, resulting in SAPO-34 crystals with varying properties and characteristics [9].

In the synthesis of SAPO-34 zeolite, there are several factors, including template, concentration template, crystallization time, crystallization temperature, type and/or amount of reagent sources (i.e., silica and alumina), impact the synthesis and properties of the SAPO-34 molecular sieve [10-13].

SAPO-34 zeolite membranes have been developed to effectively separate gases, specifically CO2 from CH4, [14]. Pseudoboehmite and aluminum isopropoxide are the primary sources of aluminum for SAPO-34 synthesis, while silicon is sourced from fumed silica, colloidal silica, and tetraethyl orthosilicate [15].

Numerous research groups study SAPO-34 zeolite for its potential applications, and its versatile properties make it valuable in various fields, including catalysis, adsorption, and separation processes [16-18]. Researchers continue exploring its synthesis methods, modification techniques, and applications to better understand and harness its capabilities for industrial and scientific purposes.

Our research group has published a series of studies on the preparation of membranes to treat various effluents [19-27]. This study is an integral part of this line of search. Therefore, within this context, this work aims to prepare SAPO-34 zeolite and zeolite membranes using the hydrothermal method, modifying synthesis parameters such as different silica sources to investigate the effects on the crystallization process and morphology.

2. Materials and Methods

All chemicals and solvents were purchased from commercial suppliers and used as received, including Aluminum Isopropoxide (≥98% $C_9H_{21}O_3Al$), Tetraethylorthosilicate ($SiC_8H_{20}O_4$), Colloidal

Silica (LUDOX HS-40, 40% SiO_2), Phosphoric acid (H_3PO_4, 85%), Morpholine (99% C_4H_9NO) Sigma-Aldrich and Aerosil 380 (Evonik).

2.1 Preparation of SAPO-34 Zeolite with Different Silica Sources

SAPO-34 zeolite was prepared using a two-stage hydrothermal crystallization method based on changes made to the conventional technique described by the authors [28].

The precursor reagents were added in stoichiometric proportions to obtain a reaction mixture with the following molar composition: [$1.00Al_2O_3$:$1.06P_2O_5$:$1.08SiO_2$:2.09R:$66H_2O$] where R is Morpholine (C_4H_9NO).

In the first step, phosphoric acid and water were mixed. After this dilution, aluminum isopropoxide was added slowly. Agitation was carried out with a mechanical stirrer, stirring the solution for 2 h. After 2 h, water was added and stirred vigorously for another 7 h, thus forming solution 1. Morpholine and water were added and mixed manually with the glass rod. After this procedure, the silica source was added slowly, developing solution 2. This solution 2 was added, little by little, to solution 1. After mixing the solutions, water was added, and then the reaction mixture remained under vigorous stirring for 7 h.

Hydrothermal synthesis two-stage process: The reaction mixture obtained was transferred to stainless steel autoclaves with an internal Teflon coating, which was placed in an oven at 38°C for 24 h and at 200°C for another 24 h. After this time, the autoclaves were cooled, and the solids formed were recovered by centrifugation and washed with plenty of deionized water. The product was dried in an oven at 100°C for 6 h.

2.2 Preparation of Ceramic Support

Initially, the alumina was pre-treated to remove possible contaminants from obtaining, transporting, and storing the alumina. 150 ml of dispersion was prepared under magnetic stirring for 30 min, with the following composition: 40% alumina and 60% ethanol at 50%. After shaking, it was left to rest until the two phases separated, where the ethanol with possible contaminants was removed with a pipette and then placed in the oven for 24 h at 60°C [18].

The dry product (alumina powder) was sent to the mechanical mixer together with 0.2% PABA (para-aminobenzoic acid), 0.5% oleic acid (lubricant), and 3.0% deionized water. Finally, the mixture obtained was weighed, placed in the mold, and pressed with 5 tons, giving rise to flat ceramic supports (alpha-alumina) with a disc-shaped configuration.

Using a heating rate, the ceramic supports sintering was carried out in a high-temperature laboratory furnace at 1300°C.

A polishing process was carried out to improve the adhesion and uniformity of the material layer deposited on the ceramic support's surface.

Polishing took place using the metallographic polisher model - PL02E, where the following steps were followed to carry out this process: (1) turn on the polisher; (2) add the diamond paste and spread it with a spatula; (3) open the water valve at a low flow rate; (3) hold the ceramic support lightly on top of the polishing cloth for 5 min (all procedures for handling the ceramic supports were performed using latex gloves, to avoid oily hands). After the polishing procedure, the ceramic support was cleaned using an ultrasonic bath (USC-1400 – Unique) with water to free the pores of alpha-alumina particles.

A ceramic flat membrane (alpha-alumina) was produced with a diameter of 26.6 mm and a thickness of 3.6 mm [19].

2.3 Production of SAPO-34/Alpha-Alumina Zeolite Membranes

The hydrothermal synthesis for the formation of the zeolite membrane follows the same conditions as the synthesis of SAPO-34 zeolite (section 2.1). It is synthesized under autogenous pressure by the nucleation and growth of zeolite crystals on the surface of the ceramic support (alpha-alumina).

The ceramic support (alpha-alumina) was washed in an acetone solution (1 mol/L) and dried at 60°C before use. This previously passed ceramic support was added to the SAPO-34 zeolite reaction mixture, then the product (reaction mixture + ceramic support) was placed in a Teflon crucible and inserted into a stainless steel autoclave, and placed in an oven at 38°C for 24 h and at 200°C for another 24 h. After the crystallization time had elapsed, the autoclave was removed from the range and cooled to room temperature. The SAPO-34 zeolite membrane was removed from the Teflon crucible, and the crystalline phase was separated from the aqueous solution with a Buchner funnel. The crystals were washed with distilled water and dried at room temperature. Due to the structure template (morpholine) blocking the zeolite pores, it is necessary to carry out a heat treatment in the muffle furnace at 600°C for 8 h.

2.4 Characterization

X-ray diffraction patterns were carried out on a Shimadzu XRD 6000 using Cu Kα radiation at 40 kV/30 mA, with a goniometer velocity of 2°/min and step of 0.02° in the 2θ range from 3.0° to 50.0°.

A VEGA TESCAN scanning electron microscope was used to perform microscopy on the samples. The powder samples were covered with a thin layer of gold by a metallizer and fixed to support with carbon adhesive tape.

The elemental analysis was determined through energy-dispersive X-ray spectrophotometry in a Shimadzu EDX-700 instrument.

The bubble point method was used to measure pores with a size above 50 nm and is standardized by ASTM F316-03. It measures the pressure necessary to flow a gas (air or N_2, for example) through a membrane whose pores are filled with a liquid.

Porosimetries were performed on a Micromeritics Autopore IV 9500 mercury porosimeter.

The system used to analyze the contact angle was composed of a digital photo camera Nikon D5000, positioned in front of a platform, where the membranes were placed, and a drop of deionized water was deposited on the film's surface.

The mechanical resistance of the ceramic support (alpha-alumina) was by the ASTM C158 technical standard on a universal testing machine (Instron 1000 KN EMIC). The compression test was used to evaluate the tensile strength of the ceramic support (alpha-alumina).

3. Results and Discussion

Figure 1 shows the result of the XRD analysis, with a 2θ scan between 5 and 50° of the ceramic support after grinding, shaping, uniaxial compaction, and sintering at 1300°C of the alumina.

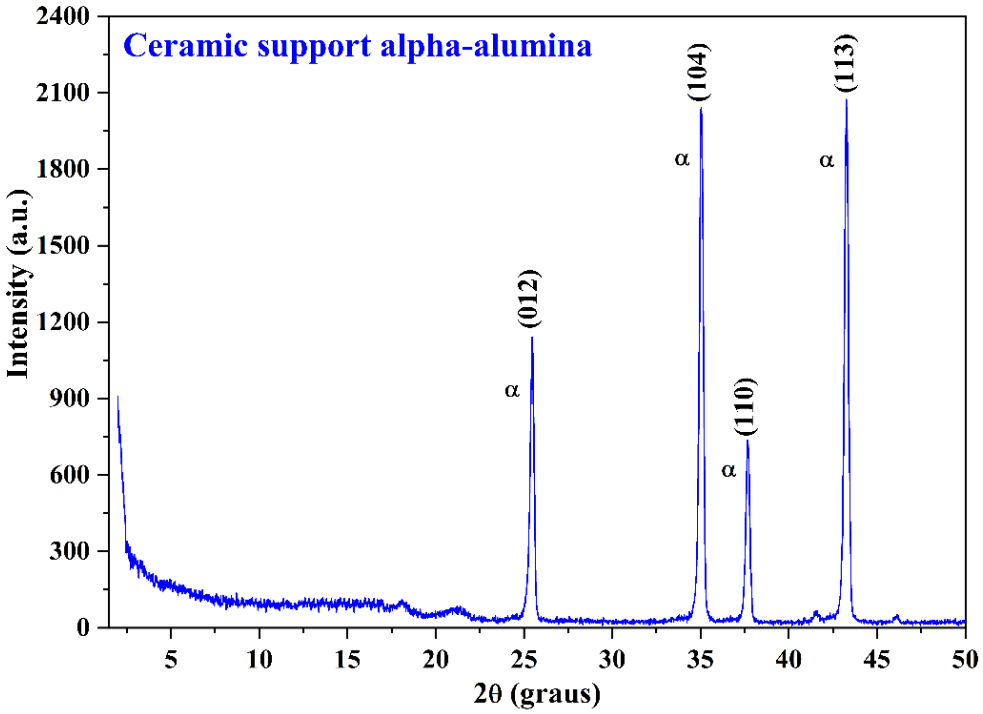

Figure 1 XRD spectra of the ceramic support obtained after grinding, shaping, uniaxial compaction, and sintering at 1300°C of alumina.

Well-defined peaks were identified in the ranges of 2θ = 25 to 45°, which are the same characteristic of the formation of the stable alpha-alumina crystalline phase, according to the standard form JCPDS Card No. 10 – 0173, corresponding to the rhombohedral structure with the space group R- 3c. The unique existence of the very crystalline phase of alpha-alumina is also observed without the presence of impurities.

Figure 2 shows a representative image of the ceramic support (alpha-alumina) obtained by scanning electron microscopy.

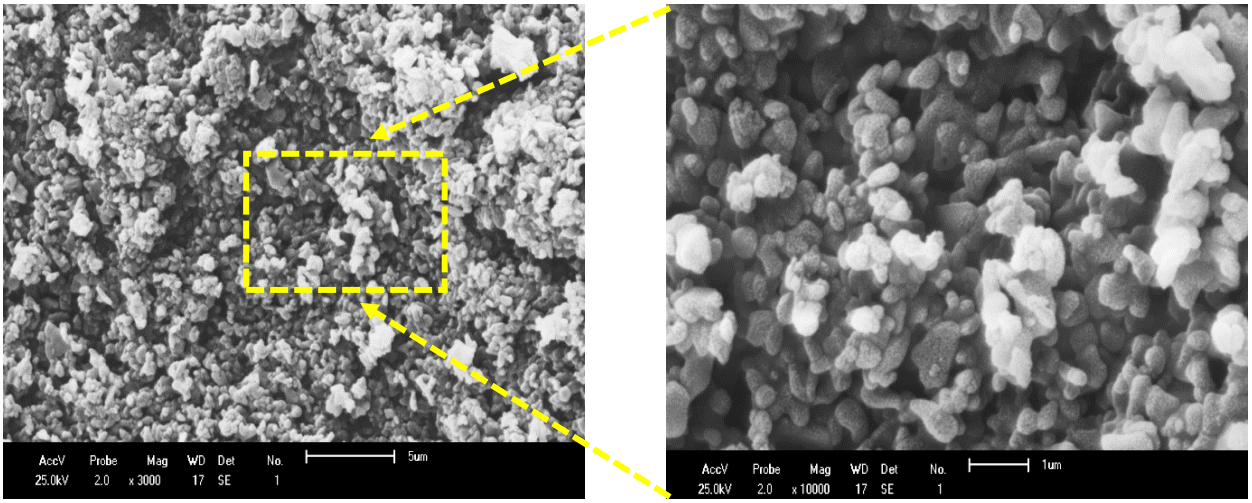

Figure 2 Micrographs of the ceramic support after grinding, shaping, uniaxial compaction, and sintering at 1300°C of alumina.

The presence of irregular particles (heterogeneous morphology) is observed in the micrographs. This is mainly due to the high particle size of the raw material used in the processing stage. It was also observed that the higher the treatment temperature, the less rough the shapes of the alumina particles. This result is in agreement with the literature [29].

Using ImageJ software, scanning electron microscopy images were used to quantify the particle size of the alpha-alumina ceramic support, as seen in the histogram in Figure 3, a cumulative distribution of particles. Measurements were taken of 25 particles from random samples, and with this image processing, it was possible to estimate the average particle size values.

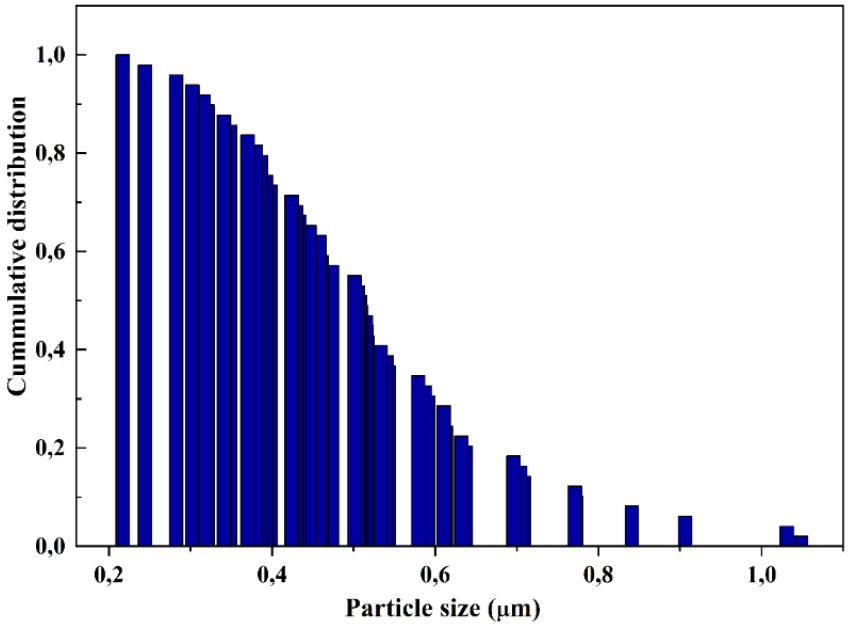

Figure 3 Normalized cumulative particle size distribution of the alpha-alumina ceramic support (with average particle size 0.539 μm).

Figure 3 displays the normalized cumulative number of particles as a function of particle size (μm). The average particle size for the ceramic support was then obtained at 0.539 μm.

The bubble point method has been one of the most widely used methods for determining membrane pore size and pore size distribution [30-32].

It is based on the principle that the pressure required to force an air bubble through a pore is inversely proportional to the size of the pore, as described by Laplace's equation:

$$r_p = 2\sigma/\Delta P \cos\theta \quad (1)$$

Where ΔP is the pressure difference across the membrane, σ the surface tension at the liquid/air interface, r_p the pore radius and cosθ contact angle between the two liquids and the membrane pore wall.

It is observed that the pore diameter predicted by the bubble point method corresponds to the alpha-alumina ceramic support (3.32 μm). Ceramic membranes (alpha-alumina) can be classified as microfiltration membranes.

The tensile strength test applies increasing uniaxial loads to a specific sample until failure. The tensile strength of the alpha-alumina ceramic support was 9.4 MPa. The alpha-alumina ceramic

support was sintered at a temperature of 1300°C, which allows for dense ceramic support due to its high sintering temperature. Thus, having less porous ceramic support, greater tensile strength is expected compared to supports with greater porosity. These results are to the literature [33].

Mercury porosimetry can be used to evaluate the pore volume distribution of membranes. The method is based on the fact that mercury is an enormously liquid substance in most materials. When mercury is forced into a dry membrane, with the volume of mercury being determined at each pressure, a cumulative volume of mercury as a function of applied pressure is established, from which the pore size distribution is deduced. The Laplace equation can describe the relationship between operating pressure and membrane pore size. This equation assumes cylindrical pores, which is generally not the case for most membranes; therefore, a morphological constant must be introduced to correct the results. During the experiment, the most prominent pores are filled with mercury at a certain minimum pressure. As the pressure increases, the smaller pores are filled until a maximum intrusion value is reached, i.e., all pores are filled. Thus, the pore size distribution of the membrane can be determined because each pressure is related to a specific pore size [34, 35].

The graph of the average pore diameter as a function of the accumulated mercury intrusion volume of the ceramic support is shown in Figure 4.

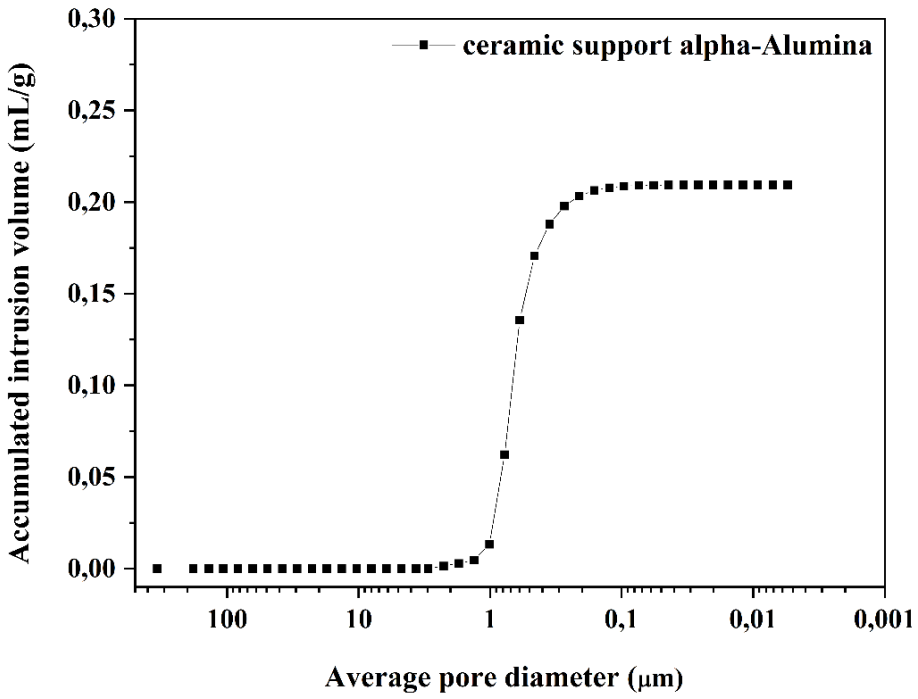

Figure 4 Graph of the average pore diameter and the volume of mercury intrusion accumulated in the ceramic support.

It is observed that the ceramic support presents most of the pore diameters varying from 2.0 to 0.4 μm, as can be seen in the slope of the curve in this range. From the curve's central intersection, we extract the average pore size equal to 0.71 μm.

Figure 5 shows the distribution graph of the average pore diameters of the ceramic support (alpha-alumina).

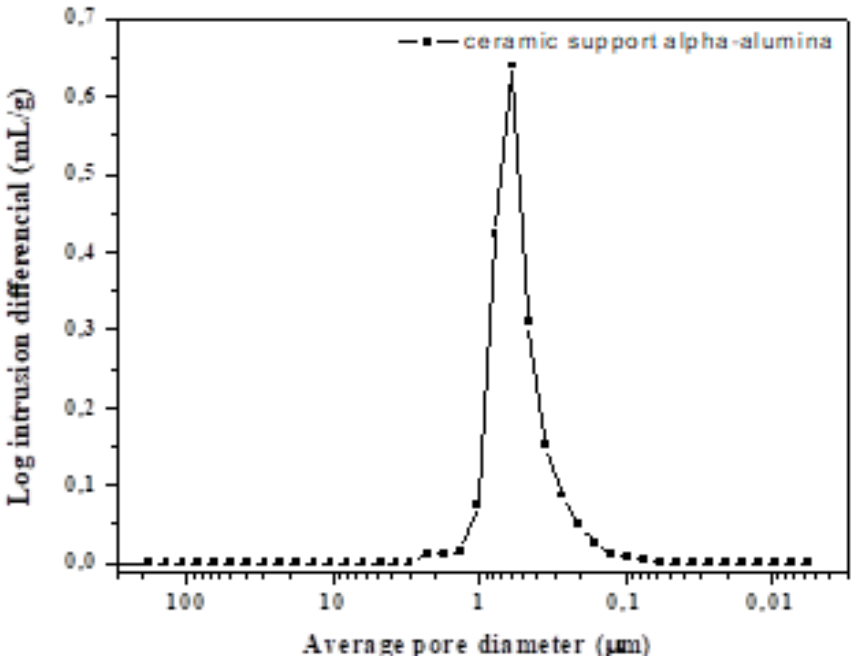

Figure 5 Graph of average pore size distribution as a function of variation in mercury intrusion volume into the ceramic support (alpha-alumina).

Figure 5 shows that the ceramic support (alpha-alumina) has an unimodal structure and a narrow distribution of pores, which is a determining factor in characterizing it as highly selective in the region of 2.0 to 0.4 µm.

According to the value found for the average pore diameter of 0.71 µm, ceramic supports (alpha-alumina) can be classified as microfiltration membranes. Due to its narrow pore size distribution range, the support likely has high selectivity in the 0.71 µm region.

The contact angle value obtained for the ceramic support was 0° due to the presence of –OH groups and the capillarity of the ceramic support on the surface [36].

It is generally accepted that angle values less than 90 degrees (q < 90°C) represent a surface with an affinity for water, called hydrophilic, that is, high affinity of water molecules towards the substrate. Values greater than 90 degrees (q > 90°C) represent a surface with lower affinity, that is, lack of attraction for water molecules, called hydrophobic surfaces. Surfaces with a contact angle with water greater than 140 degrees are called superhydrophobic surfaces [37].

The ceramic support presented a high Al_2O_3 content, proving the high purity (98.94%). The low content of impurities, such as CaO, SiO_2, and Fe_2O_3, totaling 0.84%, is significant so that they do not interfere with the synthesis of zeolite membranes and MOFs. However, alumina (Al2O3) used in industries or laboratories that produce membranes uses raw materials with a high purity content (above 99.00%).

The effect of different silica sources on the hydrothermal property of SAPO-34 is examined from the influence of final product crystallinity and morphology.

In this study, x-ray diffraction was used to confirm the presence of SAPO-34 zeolite and the purity of the samples. The analyses performed were compared with the standard IZA diffractogram that uses the result of the SAPO-34 synthesis developed by the authors [28].

In Figure 6 (a), (b), and (c), the x-ray diffractograms of the SAPO-34 samples with different silica sources (Aerosil 380, colloidal silica, and TEOS) are presented in this order.

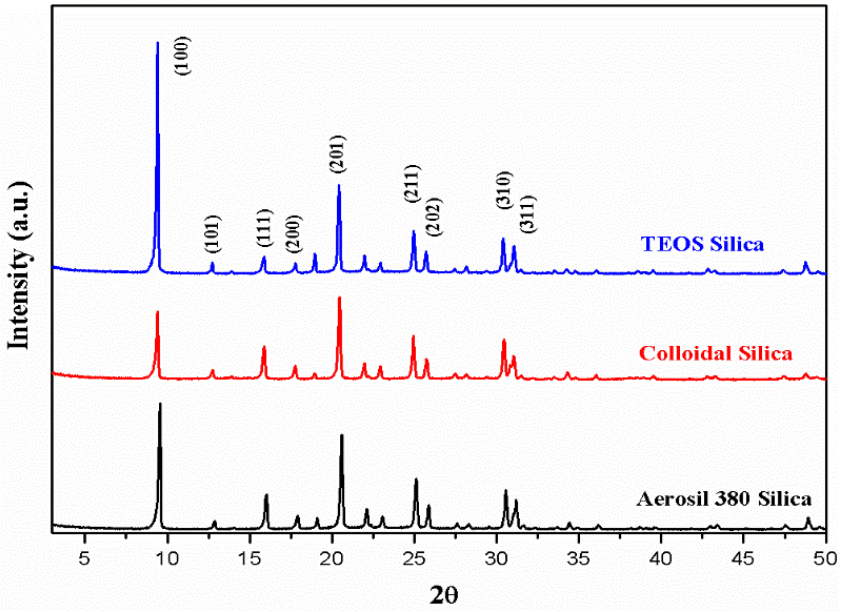

Figure 6 XRD spectra of the SAPO-34 with different silica sources: (a) Aerosil 380, (b) Colloidal Silica, (c) TEOS.

Analyzing the diffractograms (Figure 6), it is possible to verify that all materials have peaks originating from the crystalline phase of the Chabazite zeolite (CHA), which corresponds to the SAPO-34 molecular sieve, according to the (IZA) XRD pattern with some variations in the intensity of the peaks. All samples exhibit the typical diffraction pattern of pure CHA topology without impurity. The diffraction pattern matches the PDF card JCPDS Card N. 47-0617.

The phase, yield, and crystallinity of samples are listed in Table 1.

Table 1 Properties of samples.

Sample	Phase	Yield (%)	Crystallinity (%)
Aerosil 380	SAPO-34	70	100
colloidal silica	SAPO-34	69	85
TEOS	SAPO-34	70	90

It was verified that contaminating phases did not occur in the synthesis of SAPO-34, even with the change of silica sources. Many authors report the presence of a competing step in SAPO-34 syntheses as the primary contamination of the zeolite crystalline phase (AFI) that corresponds to the SAPO-5 molecular sieve. Therefore, it can be considered that the synthesis method and silica sources are suitable for synthesizing SAPO-34 zeolite membranes.

It was verified that the sample synthesized with Aerosil 380 silica presented greater crystalline intensity than the other models, suggesting the formation of a greater quantity of crystalline material belonging to the SAPO-34 molecular sieve. Meanwhile, the two samples showed lower intensity due to the lower reactivity of colloidal silica and TEOS. Similar results were found in the literature using morpholine as a template [28].

The elemental composition of the SAPO-34 zeolite reaction mixture presented in the methodology and the corresponding final composition are represented in the form of oxides (Al_2O_3, SiO_2, and P_2O_5) and the result obtained from the FRX-ED analysis presented in Table 2.

Table 2 Chemical composition of SAPO-34 zeolite obtained by the hydrothermal synthesis method using different silica as a source and analyzed by FRX-ED.

SAPO-34 zeolite	Al_2O_3(%)	P_2O_5(%)	SiO_2(%)	Others (%)	Si/Al	Al/P
Aerosil 380	38.38	37.97	23.53	0.07	0.52	1.41
Colloidal	38.35	37.92	23.51	0.06	0.52	0.52
TEOS	38.33	37.92	23.50	0.06	0.52	0.52

According to the result obtained from the FRX-ED technique of the SAPO-34 synthesis product presented in Table 2, it appears that the investigated zeolite showed an increase in the Al/P ratio to the value of the theoretical reaction mixture (Al/P = 0.83), indicating that the silicon incorporation mechanism in the prepared SAPO-34 structure occurred relatively through phosphorus substitution, producing a hydroxyl group forming a bridge between Si and Al (–SiOHAl–). However, it is possible to double the replacement of adjoint aluminum and phosphorus with two silicon atoms to increase the Si/Al ratio. These two mechanisms were reported by authors [1, 7, 38].

Other oxides below 0.1% in the zeolite composition do not cause changes in its properties and are considered impurities. However, it is worth noting that these impurities may come from sample preparation for FRX-ED analysis.

Results obtained from Scanning Electron Microscopy for SAPO-34 materials with different silica sources (Aerosil 380, colloidal silica, and TEOS) can be observed in Figures 7 (a), (b), and (c), in this order.

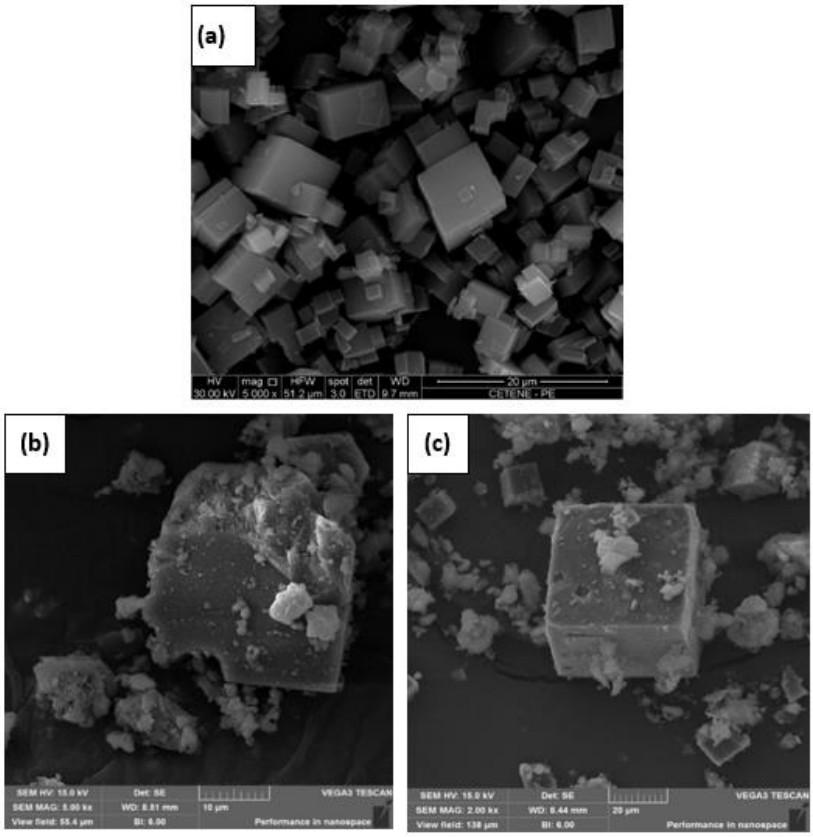

Figure 7 SEM image of SAPO-34 zeolite with different silica sources: (a) Aerosil 380, (b) colloidal silica, (c) TEOS.

Regarding the morphology of the SAPO-34 molecular sieve synthesized with colloidal silica and TEOS (Figures 7 a and d), it can be seen that it did not obtain the expected morphology, in which the crystals from the zeolite synthesis with colloidal silica showed the worst formation of the SAPO-34 structure. In the same way that the synthesis with TEOS obtained an improvement in morphology, however, few crystals were wholly formed.

From these micrographs, the crystals do not have a well-defined cubic morphology. A tendency can be seen in forming the SAPO-34 zeolite structure. However, even if the morphology is not included with the colloidal silica and TEOS sources, their respective diffractograms confirm that the synthesized material is SAPO-34. Therefore, the hypothesis of synthesizing the SAPO-34 zeolite membrane was not ruled out.

Aerosil 380 achieved the best crystallinity by forming the perfect cubic structure, unlike the other two silica sources. Based on these results, the Aerosil 380 silica source has a better formation on the SAPO-34 zeolite membrane.

These changes in morphology revealed that the effect of different silica sources plays a crucial role in controlling the shape and size of SAPO-34 crystals due to different solubility rates and reactivity of the silica sources. The same phenomenon that the silica source influences the particle size of the SAPO-34 zeolite has already been reported by authors [13] who demonstrate that the crystals formed using TEOS as a silica source are much smaller than those obtained by other sources of silica, using other synthesis conditions.

In Figure 8 (a), (b), and (c), the diffractograms of SAPO-34 zeolite membranes from different silica sources (Aerosil 380, colloidal silica, and TEOS) are presented. All XRD patterns correspond to the chabazite structure [39], which is the typical structure of SAPO-34 zeolite. The peaks agree with SAPO-34 diffractograms (XRD) reported in the literature [2, 40-42].

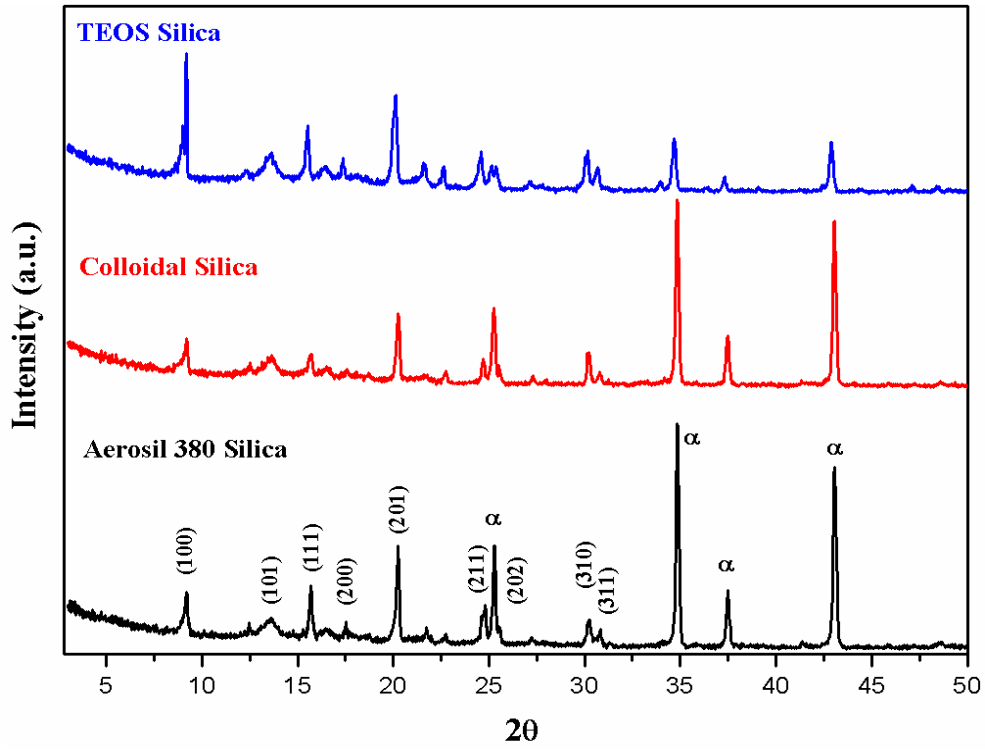

Figure 8 XRD spectra of the SAPO-34 zeolite membrane with different silica sources: (a) Aerosil 380, (b) Colloidal Silica, (c) TEOS.

In the diffractograms of the zeolite membranes (SAPO-34/alpha-alumina) obtained through the hydrothermal synthesis method, the presence of the crystalline phase of the SAPO-34 zeolite was observed, according to the results presented in Figure 6. It was also possible to keep the company of characteristic peaks of alpha-Al_2O_3 at 2θ = 25-45°, according to the standard JCPDS Card N. 10 - 0173. The diffractogram of the alpha-Al_2O_3 ceramic support was previously presented in the ceramic supports section.

The formation of the characteristic peaks of SAPO-34 zeolite and those of alpha-alumina confirmed the construction of the zeolite membrane structure (SAPO-34/alpha-alumina), regardless of the silica source used.

In Figure 9 (a), (b), and (c), some images obtained from scanning electron microscopy (SEM) corresponding to SAPO-34 zeolite membranes synthesized from hydrothermal synthesis with three different silica sources are presented: Aerosil 380 silica, colloidal silica, and TEOS.

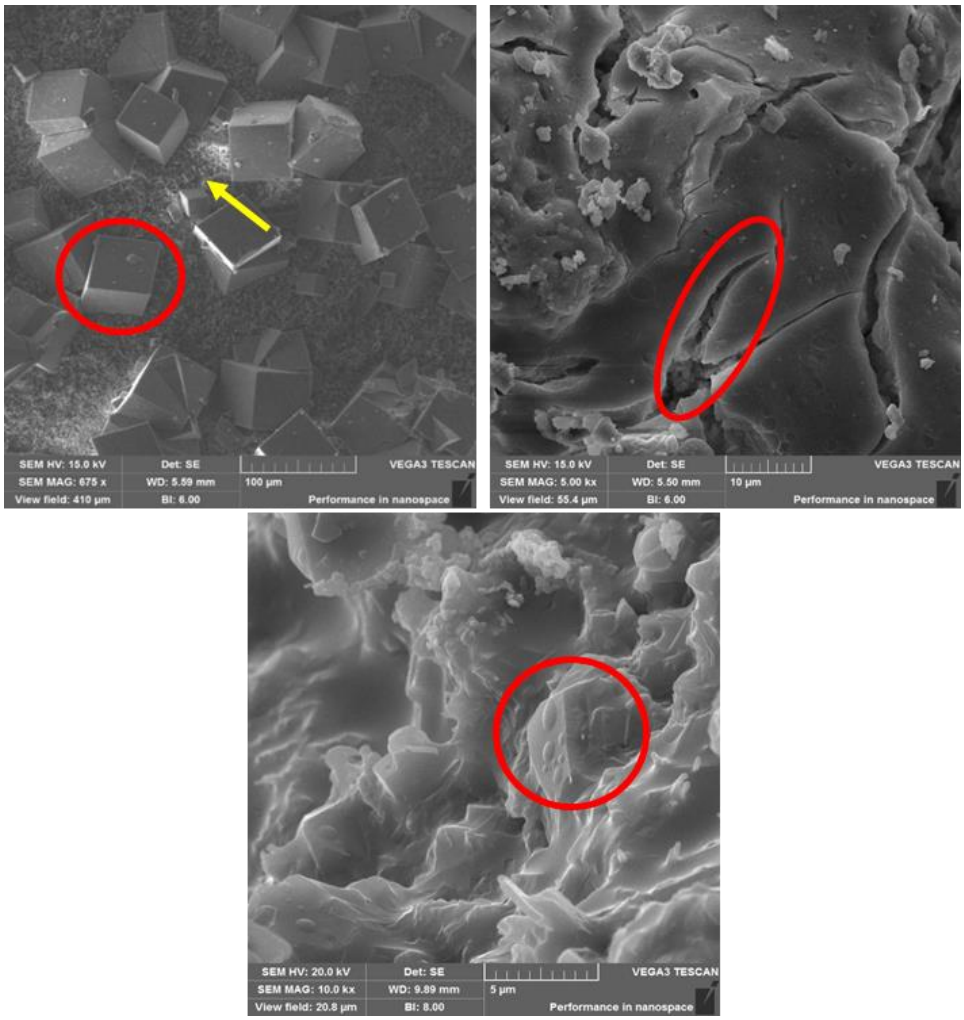

Figure 9 Scanning electron microscopy images of SAPO-34 zeolite membranes from different silica sources: (a) Aerosil 380, (b) Colloidal silica, and (c) TEOS.

The microscopies present images of SAPO-34 zeolite membranes obtained from different silica sources and a hydrothermal synthesis two-stage process.

It is observed that the surface images of the synthesized membranes (Figure 9 (a), (b), and (c)) showed zeolitic materials with different morphologies.

Aerosil 380 Silica: The SEM image of the membrane surface (Figure 9 a) shows large SAPO-34 zeolite cubic crystals evident (approx. 60 µm in diameter – red circle). However, it is noticeable that the alpha-alumina support has a homogeneous layer of SAPO-34 particles approximately 1 µm in diameter (yellow arrow).

Colloidal silica: microscopy of the membrane surface (Figure 9 b) shows cracks (intercrystalline defects - red circle) in the zeolite membrane, defects in the order of micrometers. The cubic morphology of SAPO-34 was not identified on the surface of the zeolite membrane.

However, XRD and SEM can only indicate whether a synthesized zeolite membrane was formed on the support but cannot confirm the quality of the zeolite membrane. The authors [43] reported that the primary sources of non-zeolitic pores result from the membrane layer's cracks and defects. The leading cause of damage is the lack of good adhesion between the zeolite layer and the alpha-alumina support layer.

TEOS: The SEM image of the membrane surface (Figure 9 c) reveals a dense and homogeneous layer of SAPO-34 on the alpha-alumina support without the appearance of defects or cracks. The densification of particles characterizes the morphology of SAPO-34. However, the visualization of edges and vertices of the cubic morphology of chabazite (CHA) is notable (red circle).

Table 3 presents the most critical data reported in the literature on the syntheses of zeolite membranes (SAPO-34/support).

Table 3 Summary of the most essential data reported on SAPO-34 zeolite membrane syntheses.

Synthesis conditions/Method	**Silica source/Template**	**Type of support**	**Morphology**	**Ref.**
185°C 20 h In situ Crystallization	Colloidal/TEAOH	alpha-alumina	cubic zeolite crystals	[40]
170°C 48 h a 120 h Hydrothermal	Colloidal/Morpholine	Clay-alumina	cubic zeolite crystals	[43]
220°C 24 h Rubbing	Colloidal/TEAOH	Stainless steel	pseudo-cubic plate	[44]
38°C 24 h 200°C 24 h Hydrothermal two-stage process	Aerosil 380 Colloidal TEOS/Morpholine	alpha-alumina	zeolite cubic crystals cracks intercrystalline defects a dense and homogeneous layer of SAPO-34	This work

It is clear from the results presented in Table 3 that the morphology depends on the source of silica used to prepare the zeolite membrane. It is also evident that the morphology depends on several synthesis factors, such as direction, crystallization time, temperature, and type of support.

4. Conclusions

The primary aim of this study was to synthesize SAPO-34 and zeolite membranes under different sources of silica, exploring the impact of influential synthesis parameters on product quality in terms of crystallinity, phase purity, and morphology.

The study revealed that Aerosil 380 silica is the optimal silica source for synthesizing SAPO-34 zeolites and zeolite membranes within the conditions studied. The zeolite membranes, specifically SAPO-34/alpha-alumina, exhibited a consistent and even distribution of SAPO-34 phase zeolitic crystals. The absence of defects or cracks in these membranes confirms the successful development of the SAPO-34 zeolite membrane structure.

Acknowledgments

The authors gratefully acknowledge to the Coordenação de Aperfeiçoamento de Pessoal de Nível Superior (CAPES) for the financial support.

Author Contributions

Tellys L. A. Barbosa: Investigation, Formal analysis, Writing – Original Draft; Meiry G. F. Rodrigues: Conceptualization, Formal analysis, Funding acquisition, Writing – Review & Editing.

Funding

Conselho Nacional de Desenvolvimento Científico e Tecnológico (CNPq) and Coordenação de Aperfeiçoamento de Pessoal de Nível Superior (CAPES).

Competing Interests

The authors have declared that no competing interests exist.

References

1. Lok BM, Messina CA, Patton RL, Gajek RT, Cannan TR, Flanigen EM. Silicoaluminophosphate molecular sieves: Another new class of microporous crystalline inorganic solids. J Am Chem Soc. 1984; 106: 6092-6093.
2. Li S, Falconer JL, Noble RD. SAPO-34 membranes for CO_2/CH_4 separations: Effect of Si/Al ratio. Microporous Mesoporous Mater. 2008; 110: 310-317.
3. Jhung SH, Chang JS, Hwang JS, Park SE. Selective formation of SAPO-5 and SAPO-34 molecular sieves with microwave irradiation and hydrothermal heating. Microporous Mesoporous Mater. 2003; 64: 33-39.
4. Poshusta JC, Tuan VA, Pape EA, Noble RD, Falconer JL. Separation of light gas mixtures using SAPO-34 membranes. AIChE J. 2000; 46: 779-789.
5. Carreon MA, Li S, Falconer JL, Noble RD. Alumina-supported SAPO-34 membranes for CO_2/CH_4 separation. J Am Chem Soc. 2008; 130: 5412-5413.
6. Vistad ØB, Akporiaye DE, Lillerud KP. Identification of a key precursor phase for synthesis of SAPO-34 and kinetics of formation investigated by in situ X-ray diffraction. J Phys Chem B. 2001; 105: 12437-12447.
7. Ashtekar S, Chilukuri SV, Chakrabarty DK. Small-pore molecular sieves SAPO-34 and SAPO-44 with chabazite structure: A study of silicon incorporation. J Phys Chem. 1994; 98: 4878-4883.
8. Askari S, Halladj R. Ultrasonic pretreatment for hydrothermal synthesis of SAPO-34 nanocrystals. Ultrason Sonochem. 2012; 19: 554-559.

9. Valizadeh B, Askari S, Halladj R, Haghmoradi A. Effect of synthesis conditions on selective formation of SAPO-5 and SAPO-34. Synth React Inorg Met Org Chem. 2014; 44: 79-83.
10. Askari S, Halladj R, Sohrabi M. An overview of the effects of crystallization time, template and silicon sources on hydrothermal synthesis of SAPO-34 molecular sieve with small crystals. Rev Adv Mater Sci. 2012; 32: 83-93.
11. Salmasi M, Fatemi S, Hashemi SJ. MTO reaction over SAPO-34 catalysts synthesized by combination of TEAOH and morpholine templates and different silica sources. Sci Iran. 2012; 19: 1632-1637.
12. Wu Y, Ren X, Lu Y, Wang J. Crystallization and morphology of zeolite MCM-22 influenced by various conditions in the static hydrothermal synthesis. Microporous Mesoporous Mater. 2008; 112: 138-146.
13. Yu J. Chapter 3. Synthesis of zeolites. In: Introduction to zeolite molecular sieves. Amsterdam: Elsevier; 2007. pp. 39-103.
14. Liu B, Tang C, Li X, Wang B, Zhou R. High-performance SAPO-34 membranes for CO_2 separations from simulated flue gas. Microporous Mesoporous Mater. 2020; 292: 109712.
15. Luo M, Liu M, Fu Y, Chen W, Wang B, Mao G. TEAOH-Templated SAPO-34 zeolite with different crystallization processes and silicon sources: Crystallization mechanism and MTO performance. Eur J Inorg Chem. 2020; 2020: 318-326.
16. Yu W, Wu X, Cheng B, Tao T, Min X, Mi R, et al. Synthesis and applications of SAPO-34 molecular sieves. Chem Eur J. 2022; 28: e202102787.
17. Sun Q, Xie Z, Yu J. The state-of-the-art synthetic strategies for SAPO-34 zeolite catalysts in methanol-to-olefin conversion. Natl Sci Rev. 2018; 5: 542-558.
18. Xu J, Haw KG, Li Z, Pati S, Wang Z, Kawi S. A mini-review on recent developments in SAPO-34 zeolite membranes and membrane reactors. React Chem Eng. 2021; 6: 52-66.
19. Barbosa AS, Barbosa AS, Rodrigues MG. Synthesis of zeolite membrane (MCM-22/α-alumina) and its application in the process of oil-water separation. Desalination Water Treat. 2015; 56: 3665-3672.
20. Scheibler JR, Santos ER, Barbosa AS, Rodrigues MG. Performance of zeolite membrane (ZSM-5/γ-Alumina) in the oil/water separation process. Desalination Water Treat. 2015; 56: 3561-3567.
21. Barbosa AS, Barbosa AS, Rodrigues MG. -Synthesis Of MCM-22 zeolite membrane on a porous alumina support. Mater Sci Forum. 2015; 805: 272-278.
22. Cunha RS, Mota JD, Mota MF, Rodrigues MG, Machado F. Preparation and characterization of tubular composite membranes and their application in water flow measurements. Mater Sci Forum. 2018; 912: 263-268.
23. Barbosa AS, Barbosa AS, Rodrigues MG. Contaminants removal in wastewater using membrane adsorbents zeolite Y/alpha-alumina. Mater Sci Forum. 2018; 912: 12-15.
24. Barbosa AS, Barbosa AS, Rodrigues MG. Y-type zeolite membranes: Synthesis by secondary by method and application in treatment of oily effluents. Mater Sci Forum. 2019; 958: 23-28.
25. Barbosa AS, Barbosa AS, Rodrigues MG. Influence of the methodology on the formation of zeolite membranes MCM-22 for the oil/water emulsion separation. Cerâmica. 2019; 65: 534-545.

26. Barbosa TL, Silva FM, Barbosa AS, Lima EG, Rodrigues MG. Synthesis and application of a composite NaA zeolite/gamma-alumina membrane for oil-water separation process. Cerâmica. 2020; 66: 137-144.
27. Silva FM, Lima EG, Barbosa TL, Mota JD, Cunha RS, Lima WS, et al. Synthesis of the gamma-alumina and zeolitic membranes MOR/gamma-alumina by the steam phase transport method. Braz J Dev. 2021; 7: 13917-13934.
28. Prakash AM, Unnikrishnan S. Synthesis of SAPO-34: High silicon incorporation in the presence of morpholine as template. J Chem Soc Faraday Trans. 1994; 90: 2291-2296.
29. Busca G. Structural, surface, and catalytic properties of aluminas. In: Advances in catalysis. Volume 57. London: Elsevier; 2014.
30. Sastre G, Lewis DW, Catlow CR. Modeling of silicon substitution in SAPO-5 and SAPO-34 molecular sieves. J Phys Chem B. 1997; 101: 5249-5262.
31. ASTM. Standard test method for pore size characteristics of membrane filter by bubble point and mean flow pore test. West Conshohocken, PA: ASTM International; 2003; ASTM F316-03.
32. Reichelt G. Bubble point measurements on large areas of microporous membranes. J Membr Sci. 1991; 60: 253-259.
33. Biesheuvel PM, Verweij H. Design of ceramic membrane supports: Permeability, tensile strength and stress. J Membr Sci. 1999; 156: 141-152.
34. Zeman L. Characterization of microfiltration membranes by image analysis of electron micrographs: Part II. Functional and morphological parameters. J Membr Sci. 1992; 71: 233-246.
35. Honold E, Skau EL. Application of mercury-intrusion method for determination of pore-size distribution to membrane filters. Science. 1954; 120: 805-806.
36. Chen X, Gao X, Fu K, Qiu M, Xiong F, Ding D, et al. Tubular hydrophobic ceramic membrane with asymmetric structure for water desalination via vacuum membrane distillation process. Desalination. 2018; 443: 212-220.
37. Hebbar RS, Isloor AM, Ismail AF. Contact angle measurements. In: Membrane characterization. Amsterdam: Elsevier Inc.; 2017. pp. 219-255.
38. Li L, Cui X, Lia J, Wang J. Synthesis of SAPO-34/ZSM-5 composite and its catalytic performance in the conversion of methanol to hydrocarbons. J Braz Chem Soc. 2015; 26: 290-296.
39. Szostak R. Handbook of molecular sieves: Structures. Netherlands: Springer Nature; 1992. 584p.
40. Li S, Falconer JL, Noble RD. SAPO-34 membranes for CO_2/CH_4 separation. J Membr Sci. 2004; 241: 121-135.
41. Carreon MA, Li S, Falconer JL, Noble RD. SAPO-34 seeds and membranes prepared using multiple structure directing agents. Adv Mater. 2008; 20: 729-732.
42. Heyden HV, Mintova S, Bein T. Nanosized SAPO-34 shyntesized from coloidal solutions. Chem Mater. 2008; 20: 2956-2963.
43. Das JK, Das N, Roy SN, Bandyopadhyay S. The growth of SAPO 34 membrane layer on support surface for gas permeation application. Ceram Int. 2012; 38: 333-340.
44. Venna SR, Carreon MA. Amino-functionalized SAPO-34 membranes for CO_2/CH_4 and CO_2/N_2 separation. Langmuir. 2011; 27: 2888-2894.